World Scientific
www.worldscientific.com

SnO$_2$–ZnO nanocomposite thin films: The influence of structure, composition and crystallinity on optical and electrophysical properties

E. M. Bayan[*,§], V. V. Petrov[†], M. G. Volkova[*],
V. Yu Storozhenko[*] and A. V. Chernyshev[‡]

*Faculty of Chemistry, Southern Federal University
Rostov-on-Don, Russia*

†*Institute of Nanotechnologies, Electronics, and Equipment Engineering
Southern Federal University, Taganrog, Russia*

‡*Research Institute of Physical and Organic Chemistr
Southern Federal University, Rostov-on-Don, Russia*

§ekbayan@sfedu.ru

SnO$_2$–ZnO thin films consisting of nanoscale crystallites were obtained on glass and silicon substrates by solid-phase low-temperature pyrolysis. The synthesized materials were studied by XRD and SEM methods, electrophysical and optical properties were evaluated, as well as the band gap was calculated. It was shown that regardless of the phase composition all films were optically transparent in the visible range (310–1000 nm). The nanocrystallites' minimum size, the highest activation energy of the conductivity and the smallest band gap calculated for indirect transitions were shown for a thin film 50SnO$_2$–50ZnO. It was assumed that the band gap decreasing might be attributed to the existence of surface electric fields with a strength higher than 4×10^5 V/cm.

Keywords: Zinc tin oxide; crystal structure; optical property; thin films; semiconductors; nanocomposite.

1. Introduction

Nanoscale semiconductor films are used in almost all areas of modern industry.[1,2] Since films based on zinc oxide and tin (IV) oxide are optically transparent, stable and non-toxic,[3] they are promising materials for gas sensors,[4] solar cells and photocells,[5–7] photocatalysts,[8] etc.

Zinc oxide and tin dioxide are of great scientific interest using jointly due to the different synergetic effects.[9,10] The high stability of both pure zinc and tin oxide materials and composites based on them, as well as the conduction band formed by spherical symmetric s-orbitals of both metals, cause the occurrence of unique optical, electrophysical and other properties.[9,11] The synthesis of composite materials based on zinc[12] and tin (IV) oxides[13] in order to study the gas-sensitive properties is also particularly promising. In this case, the surface conductivity can change due to the barrier value at the two phase's interface, which occurs due to the ZnO/SnO$_2$ heterojunctions. If the metals exist in the reduced form, Schottky barriers can also be formed.[14] The presence of heterojunctions and Schottky barriers can lead to improved gas-sensitive properties.[14,15]

The properties of the obtained nanomaterials are affected by the synthesis conditions, among which the most significant is the concentration of modifying additives and temperature treatment. Zinc oxide films doped with tin in small concentrations (0, 5, and 7 at.%), formed by reactive magnetron sputtering without intentional substrate heating or cooling retain a wurtzite-type crystal structure and have similar optical properties to pure zinc oxide. However, films doped with high concentrations of tin (more than 15 at.%) have an amorphous structure[16]; film's transparency changed insignificantly.

Thin films of ZnO–SnO$_2$ were deposited on glass substrates[17] by the flash evaporation technique and annealed in a vacuum at 450°C. It was found that the tin concentration increasing (Zn:Sn = 100:0; 90:10; 70:30; 50:50) leads to the changing of hexagonal wurtzite crystal structure (Zn:Sn = 100:0; 90:10) to the Zn$_2$SnO$_4$ cubic (Zn:Sn = 70:30) and also to the particle size increasing. The material (Zn:Sn = 50:50) had a polycrystalline cubic structure of Zn$_2$SnO$_4$. For ZnO–SnO$_2$ films synthesized by spray pyrolysis technique and calcined at 500°C, an increase in the Sn^{4+} concentration from 50% to 75% leads to the transmission coefficient increasing from 0.7 to 0.95 within the visible range (400–800 nm) due to the film thickness and structural defects decreasing.[18,19] When the tin concentration increases, also the band gap increasing

§Corresponding author.

was found. For material with composition Zn:Sn = 50:50, the minimum band gap of 3.6 eV was marked.

For composite film materials based on SnO_2 doped with Zn^{2+} synthesized by spray pyrolysis, the highest transparency was achieved when small concentrations of zinc oxide (Zn:Sn = 20:80) were used.[20] When Zn/Sn ratio was close to 1, the crystallization process was blocked, which leads to the creation of the defective structure.

If the molar ratio Zn:Sn increases up to 5:1 for materials synthesized by the sol–gel method and annealed at 500 °C, a decrease in the film transparency (up to 55%) in the wavelength range 400–800 nm was observed. For materials with the Zn:Sn ratio equal to 1:1, this value was 81%.[21] The band gap energy was close to the energy of pure ZnO (3.21 eV).

Different structural transitions are noted,[22] when the annealing temperature increases: zinc–tin oxide films formed by the sol–gel method retained the spinel structure Zn_2SnO_4 up to 700 °C; up to 800 °C, the perovskite form of zinc stannate $ZnSnO_3$ was recorded. For all synthesized materials, regardless of their composition, a high transparency (80–96%) in the visible wavelength range was shown. The materials band gap at the annealing temperature 500–800 °C was 3.6 eV for the Zn_2SnO_4 and 3.7–3.9 eV for the $ZnSnO_3$ phase, which consists of the calculated theoretical values.

During the study of ZnO–SnO_2 films synthesized by the sol–gel method, the authors showed the properties dependence on the number of deposited layers, films thickness and the annealing temperature. When the annealing temperature increases up to 600 °C, the optical transparency of double-layer films with a thickness of 110 nm reached the best value — 93%. As the film thickness increases from 110 to 270 nm, the band gap decreases from 3.85 to 3.1 eV. With the annealing temperature increasing from 400 °C to 700 °C, the band gap decreases from 3.6 to 3.15 eV, which consists of the previous results.[23,24]

The highest transparency was shown for thin ZnO–SnO_2 films synthesized by the sol–gel method and calcined at 450 °C.[25] An increase in the calcination temperature from 450 °C to 550 °C leads to a decrease in the band gap for the material Zn:Sn = 60:40 (3.19 eV). The highest value (3.28 eV) was shown for materials Zn:Sn = 70:30 and Zn:Sn = 60:40, calcined at 450 °C.

It was shown that due to the structural lattice disorder,[26,27] there is a decrease of both the band gap and the transparency in the visible wavelength range (420–800 nm).

Previous studies[28] have also shown that ZnO thin films can be obtained by our group via a new method of low-temperature solid-phase pyrolysis. Structural analysis showed that obtained films were polycrystalline with wurtzite structure. The films consist of nanocrystallites (the average particle size is about 10–20 nm) which are evenly distributed over the substrate surface and the film thickness. This method allows to obtain homogeneous nanocrystalline films with controlled thickness by the number of applied layers. Also, low-temperature solid-phase pyrolysis is more cost-effective than others, such as hydrothermal synthesis and magnetron sputtering, because it does not involve expensive equipment using. In addition, ZnO–SnO_2 nanocomposite films with a sufficient degree of crystallinity were obtained by this method.[29] At the same time, the optical properties of these materials have not been sufficiently studied.

Thus, the aim of this work is a more comprehensive study of the optical and electrophysical properties of composite film materials based on zinc oxide and tin dioxide synthesized by solid-phase low-temperature pyrolysis.

2. Experimental

2.1. *Materials*

For the SnO_2–ZnO thin films synthesis zinc acetate dihydrate ($Zn(CH_3COO)_2 \cdot 2H_2O$), tin (IV) chloride pentahydrate ($SnCl_4 \cdot 5H_2O$), acetone, 1,4-dioxane, distilled water and organic acid were used. All chemicals used were of analytical grade or of the highest purity available, were purchased from "ECROS", Russia. The film materials were obtained on glass and silicon substrates.

2.2. *Preparation of materials*

First, organic salts of tin and zinc were obtained from the melt. The intermediates were then dissolved in dioxane to produce materials with a molar ratio of Sn:Zn equal to 5:95, 1:1, 95:5. The resulting solution was applied three times by pouring on pre-prepared and cleaned substrates, dried first at room temperature, and then at 100 °C. The heat treatment was carried out in a muffle furnace. The heating rate of the furnace was 10 °C/min. Thermal exposure was carried out for 2 h at 550 °C. The synthesis conditions were selected based on the previous studies.[29,30] After the heat treatment, the films were gradually cooled to room temperature together with the muffle furnace. Obtained thin films materials with Sn:Zn ratio equal to 5:95, 1:1 and 95:5 will be named as material $5SnO_2$–$95ZnO$, $50SnO_2$–$50ZnO$ and $95SnO_2$–$5ZnO$, respectively.

2.3. *Characterization*

X-ray diffraction analysis (XRD, ARLX'TRA diffractometer, Thermo ARL on CuKa radiation) was used to study the obtained materials. The phase composition analysis was performed using the Crystallography Open Database (COD). The quality of the films, the thickness and size of the nanocrystallites in the volume and on the surface were controlled by scanning electron microscopy (SEM, Nova Nanolab). The software Image J and Digimizer are used to measure the particle diameter. The optical properties of film materials applied on the glass substrates were studied using optical absorption spectra obtained on a Varian Cary-100 spectrophotometer in the wavelength range of 300–1100 nm.

The average particle size D was calculated using the Scherrer equation: $D = k \cdot \lambda/(\beta \cdot \cos\Theta)$, where λ is the

wavelength of the copper X-ray radiation (1.5406 Å), β is the full width at the half maximum of the diffraction peak, θ is the diffraction angle, and k is the particle shape factor (for spherical particles, $k = 0.9$).

To study the electrophysical properties, V–Ni metal contacts with a thickness of 0.2–0.3 microns were formed on top of films by vacuum thermal deposition, the distance between the contacts was 1 mm. It was measured using an automated installation for determining the parameters of gas sensors at the Center for Collective Use "Microsystem Technics and Integral Sensors".[30] The error of measurements by the device, taking into account temperature fluctuations within one measurement, can be estimated at 0.1%.

The band gap energy was found according to absorption edge analysis.[31]

3. Results and Discussion

3.1. *X-ray diffraction*

The results of XRD analysis showed that all materials are nanoscale (Fig. 1), have a crystal structure of the wurtzite (material $5SnO_2$–$95ZnO$) and cassiterite (material $95SnO_2$–$5ZnO$). The X-ray pattern of the $50SnO_2$–$50ZnO$ material (curve 2) contains peaks characteristic of both the wurtzite (COD ID 2300450[32]) and cassiterite (COD ID 1521419[33]) structures, but the intensity is slightly lower than that for the $5SnO_2$–$95ZnO$ and $95SnO_2$–$5ZnO$ materials. Thus, it can be concluded that the material 50Sn-ZnO is a mixture of two phases and does not form a new compound. The ratio of the crystalline and amorphous phases was calculated from the XRD data. The material $5SnO_2$–$95ZnO$ has a crystallization (67%), which is confirmed by the highest peak intensity.
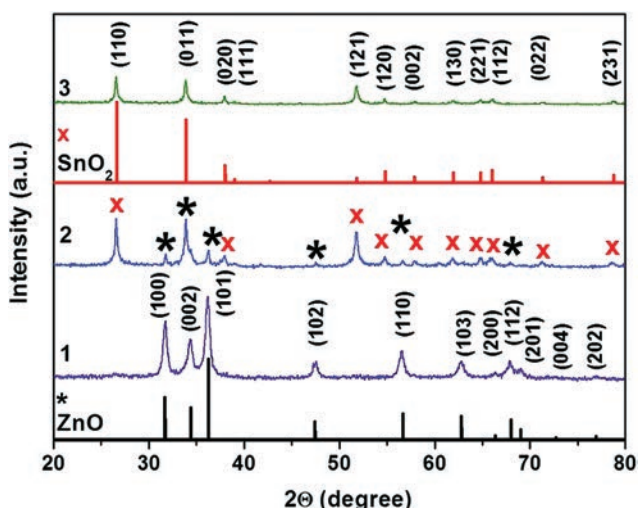

Fig. 1. XRD pattern of obtained materials calcined at 550°C: $5SnO_2$–$95ZnO$ (curve 1), $50SnO_2$–$50ZnO$ (curve 2), $95SnO_2$–$5ZnO$ (curve 3), ZnO (COD ID 2300450[32]) and SnO_2 (COD ID 1521419[33]).

The $95SnO_2$–$5ZnO$ material is characterized by the lowest peak intensity compared to other materials, which may indicate a greater amorphous component for materials based on tin (IV) oxide, which is confirmed by the calculation of the crystallinity degree (64%) and is in good agreement with other studies.[16,18] The highest degree of crystallinity was observed for the composite material $50SnO_2$–$50ZnO$ (77%), which may be caused by its polycrystalline structure. The calculation of the average particle sizes according to the Scherer equation showed that the minimum particle size (15 nm) is observed for the materials $5SnO_2$–$95ZnO$ and $50SnO_2$–$50ZnO$, the average particle size for the material $95SnO_2$–$5ZnO$ is 18 nm.

3.2. *SEM analysis*

According to SEM data, the obtained film materials have a uniform surface morphology. Nanocrystallites are evenly distributed over the film surface (Fig. 2).

The thickness of the film coating formed by 3-times application of the precursor solution is about 200 nm (Figs. 2(a), 2(c) and 2(e)). Despite the fact that the films were formed during the deposition of three layers, no boundaries were observed on their SEM images. This indicates the possibility of the mixed zinc and tin (IV) oxides films thickness controlling by layer-by-layer deposition in the range 30–200 nm. By statistical SEM analysis, it was shown that the sizes of metal oxide nanoparticles are in the range from 4 to 32 nm (Figs. 2(b), 2(d) and 2(f)) in different ratios depending on the material composition. For the $50SnO_2$–$50ZnO$ thin film, the largest size distribution of crystallites is noted, but about 50% of the crystallites have a size of less than 12 nm, and the maximum number (37%) of crystallites have sizes from 8 to 12 nm (Fig. 2(d)). For the $5SnO_2$–$95ZnO$ and $95SnO_2$–$5ZnO$ thin films, the main fraction is crystallites with sizes of 12–16 nm — about 61% in both cases. The number of crystallites with sizes less than 12 nm for the material $5SnO_2$–$95ZnO$ is 25%, and for the material $95SnO_2$–$5ZnO$ — 15%. The average crystallite sizes determined by SEM studies were 13, 12, and 16 nm for the $5SnO_2$–$95ZnO$, $50SnO_2$–$50ZnO$, and $95SnO_2$–$5ZnO$ thin films, respectively. Thus, using solid-phase low-temperature pyrolysis, it is possible to form thin nanoscale films of mixed zinc and tin (IV) oxides with particle sizes, on average, from 8–16 nm.

3.3. *Electrophysics*

The analysis of the observed results showed that the generation of charge carriers as a result of thermal excitation is of an activation nature, so, the dependence of the material resistivity on the temperature is described by the Arrhenius equation[31]:

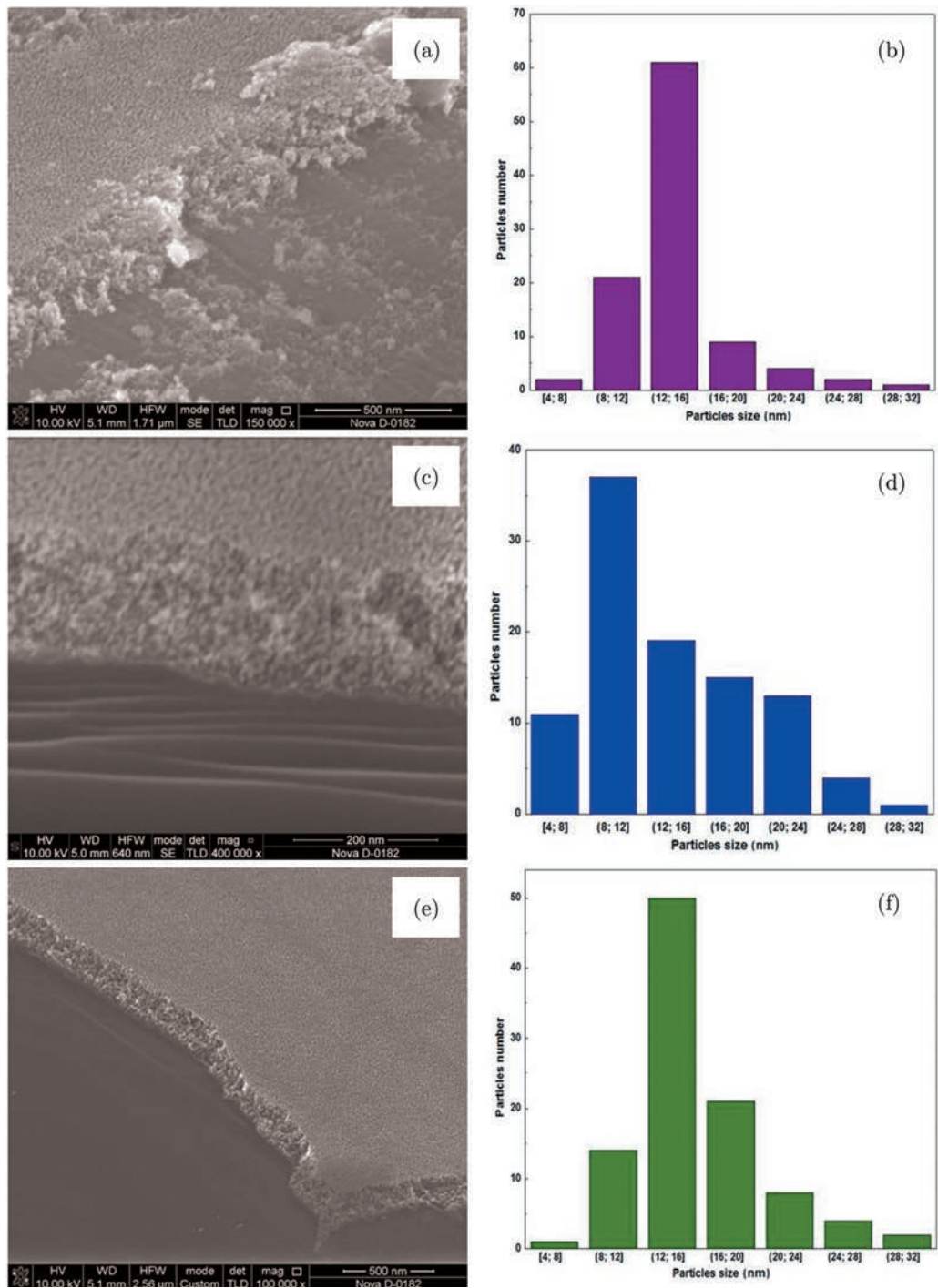$$\rho = \rho_0 \cdot \exp(E_a / k \cdot T),$$

Fig. 2. SEM images of surface and particle size distribution for materials calcined at 550 °C: $5SnO_2$–95ZnO (a, b), $50SnO_2$–50ZnO (c, d) and $95SnO_2$–5ZnO (e, f).

where E_a is the activation energy of the conductivity, k is the Boltzmann constant, and ρ_0 is the pre-exponential factor (constant).

The calculated activation energy (E_a) of the conductivity was estimated based on the Arrhenius equation, for temperature ranges in which a linear decrease in resistance is observed (approximately from 100–150 to 250–300 °C). Dependence of the activation energy on the Sn:Zn ratio for SnO_2–ZnO thin films of adjustable thickness is shown in Table 1.

Table 1. Characteristics of SnO₂–ZnO films obtained by solid-phase low-temperature pyrolysis.

Material	5SnO₂–95ZnO	50SnO₂–50ZnO	95SnO₂–5ZnO
E_a, eV	0.94	1.24	1.07
E_{g1}, eV	3.32	3.78	3.90
E_{g2}, eV	3.11	2.98	3.23; 3.50
D (XRD), nm	15	15	18
D (SEM), nm	13	12	16

Notes: E_{g1} — band gap for direct transitions.

E_{g2} — band gap for indirect transitions.

Fig. 4. Optical absorption spectra of materials calcined at 550 °C: 5SnO₂–95ZnO (curve 1), 50SnO₂–50ZnO (curve 2) and 95SnO₂–5ZnO (curve 3).
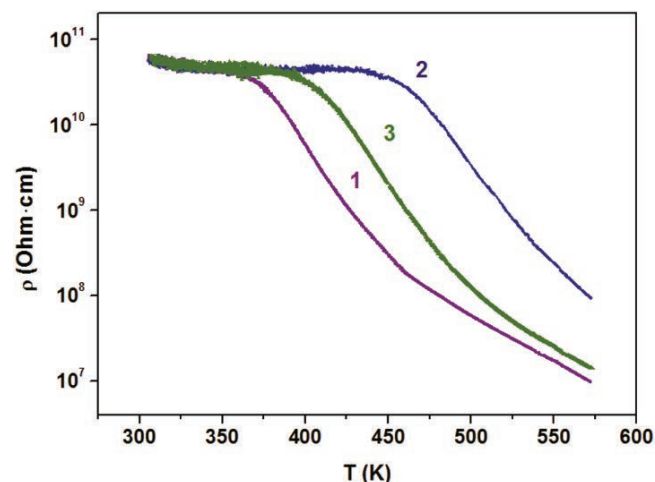

Fig. 3. Resistance (ρ) dependences on temperature of materials calcined at 550 °C 5SnO₂–95ZnO (curve 1), 50SnO₂–50ZnO (curve 2), 95SnO₂–5ZnO (curve 3).

Resistance (ρ) dependences on temperature for synthesized materials is shown on Fig. 3.

One can note that the value of the conductivity activation energy affects the temperature at which the film resistivity begins to decrease, as well as the value of the resistivity. At a higher E_a, the decrease in the value of p begins at a higher temperature, and the value of p at high heating temperatures is also proportional to the value of E_a. One also can note that there is a correlation between E_a and the particle size calculated from the XRD. The lower conductivity activation energy is characterized by lower values of nanocrystallites' size.

3.4. Optical properties

Regardless of the material composition, the transparency of all films is above 90% in the wavelength range of 310–1000 nm. The maximum absorption coefficient was observed for material 95SnO₂–5ZnO in the range of 290–300 nm (Fig. 4).
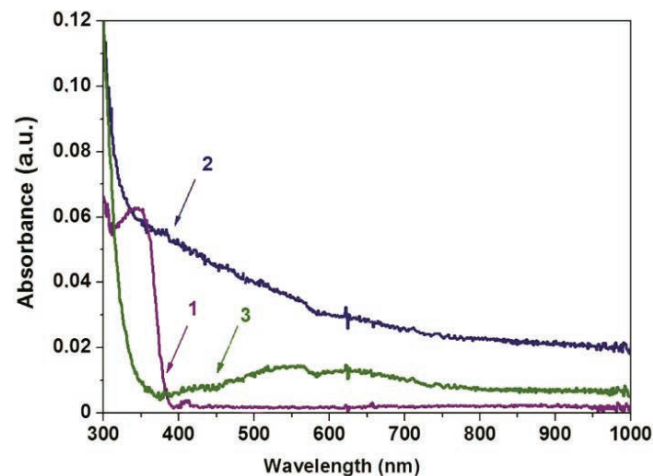
From the optical absorption spectra, it is possible to calculate the band gap E_{g1} of semiconductor materials. Then, the dependence of the absorption coefficient α on the wavelength λ will be determined by the following equation[31]:

$$\alpha = A(h\nu - E_{g1})^{1/2},$$

where h is the Planck constant, v is frequency of optical radiation and A is constant.

At the same time, in complex semiconductors, which include metal oxides, indirect transitions can occur.[31] For these materials, the dependence of the absorption coefficient on the photon energy is more complex, which in general can be described by the following function:

$$\alpha^{1/2} = f(h\nu), \quad \text{if } \Delta E_g - E_p < h\nu < \Delta E_g + E_p,$$

where E_p is the photon energy, that is absorbed or emitted during indirect transitions.

Extrapolating the smaller part of the dependence $\alpha^2 = f(h\nu)$ and (or) $\alpha^{1/2} = f(h\nu)$ to the zero X-axis allows to determine the value of the band gap for direct and indirect transitions. In this case, the dependences $\alpha^{1/2} = f(h\nu)$ can be extrapolated by several straight lines. The line 1 corresponds to the dependence $\alpha^{1/2}$, which intersects with the X-axis at the point $(\Delta E_g + E_p)$. The line 2 characterizes the dependence $\alpha^{1/2}$ and intersects with the X-axis at the point $(\Delta E_g - E_p)$. The length of the section between the specified points of lines and X-axis intersection is equal to $2E_p$. The point in the middle of this section will be equal to E_{g2}.

The analysis of Tauc plot presented in Fig. 5 shows that for SnO₂–ZnO films the band gap is determined by indirect transitions. So, for film with composition 5SnO₂–95ZnO, the band gap is 3.32 eV (Fig. 5(a)) determined from the dependence for direct transitions $\alpha^2 = f(h\nu)$ and 3.11 eV (Fig. 5(b)) determined from the dependence for indirect
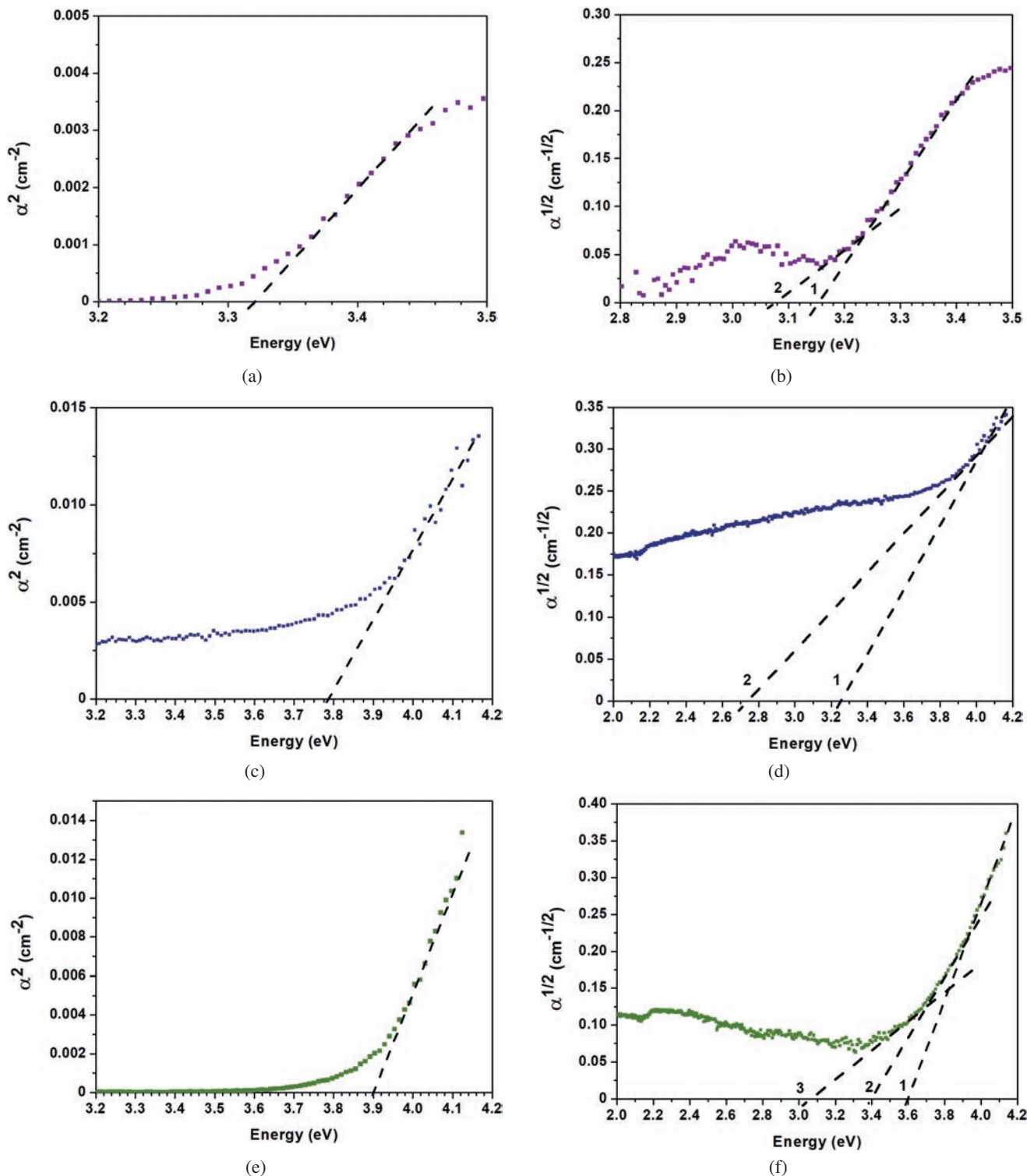
(a)

(b)

(c)

(d)

(e)

(f)

Fig. 5.   Determination of the band gap for materials calcined at 550 °C 5SnO$_2$–95ZnO (a, b), 50SnO$_2$–50ZnO (c, d), 95SnO$_2$–5ZnO (e, f) for direct (a), (c), (e) and indirect transitions (b), (d), (f).

transitions $\alpha^{1/2} = f\,(h\nu)$. This difference is even greater for composite material 50SnO$_2$–50ZnO: E_{g1} is 3.78 eV and 2.98 eV, respectively (Figs. 5(c) and 5(d)). For the film 95SnO$_2$–5ZnO the band gap determined from direct transitions is 3.90 eV (Fig. 5(e)), and for indirect transitions, two can be distinguished — between straight lines 1 and 2 and straight lines 2 and 3. In the first case, the band gap is 3.50 eV, and in the second 3.23 eV (Fig. 5(f)).

It is known that the crystallites' size affects the film's physical properties. For example, the optical band gap measured in a thin SnO_2 film with a fine-grained structure (11–19 nm) differs significantly from the band gap of SnO_2 single crystals (3.54 eV) and is close to 3 eV.[34] The authors explain this both as the non-stoichiometric composition of the film and the presence of band tails caused by the high defect concentration. Apparently, in films based on a mixture of two oxides, there may be local regions in which there will be different band gap, determined by different ZnO or SnO_2 oxides. This is also indicated by the presence of a sufficiently large absorption for energies below the band gap (the Urbach tail), which can be calculated according to the Urbach rule.[35]

$$\alpha = \alpha_0 \exp(E - E_g)/E_0,$$

where α_0 is constant, $1/E_0$ is the Urbach slope, which characterizes the steepness degree of the absorption coefficient dependence; it depends on the material parameters.

It was shown[36] that at room temperature, structural disorder due to grain boundaries and other structural defects is the dominant contribution to the Urbach tail. At the same time, the existence of different materials local regions will lead to the appearance of heterojunctions and chaotically directed electric fields, in which the Keldysh–Frantz effect can occur.[34]

The calculation of the E_0 value allows to estimate the degree of disorderliness, as well as the presence of a surface electric field. For the $5SnO_2$–$95ZnO$, $50SnO_2$–$50ZnO$ and $95SnO_2$–$5ZnO$ thin films, the calculated value of E_0 was 0.05, 2.95 and 0.22 eV, respectively. E_0 value for $5SnO_2$–$95ZnO$ is only 5 times higher than 0.01 eV, which is typical for these material types; in contrast, for materials $50SnO_2$–$50ZnO$ and $95SnO_2$–$5ZnO$ this excess is 295 and 22 times, respectively. Analysis of the crystallite sizes from SEM images showed that the material $50SnO_2$–$50ZnO$ is the most structurally disordered material. At the same time, the significantly different value of E_0 suggests the presence of a surface electric field in this material. In particular, the presence of a strong surface electric field is discussed in the work.[37] The authors used electrostatic force microscopy to show that the charge is localized at the grain boundaries. The existence of local bending zones at the grain boundaries of SnO_2–ZnO films was experimentally confirmed. The potential spread between neighboring grains could reach 40 mV. At a distance between the grains of 1 nm or less, this gives an electric field strength higher than 4×10^5 V/cm. At this magnitude of intensity, the electric field-stimulated tunneling of charge carriers generated by optical radiation occurs, which leads to a decrease in the band gap.[34] As one can see, in the $50SnO_2$–$50ZnO$ film, the Urbach tail is most noticeable, which on the one hand may be a consequence of structural disorderliness, and on the other hand, the existence of surface electric fields. This reduces the band gap to 2.98 eV for indirect transitions, compared to 3.78 eV for E_{g1} calculated from direct transitions.

In the film with the highest tin oxide concentration ($95SnO_2$–$5ZnO$), the structural disorder estimated by the calculated degree of crystallinity, is close to the film ($5SnO_2$–$95ZnO$), but the fluctuations of the surface electric field are also large. This conclusion is drawn by the observed decrease in the band gap due to indirect transitions to 3.23 eV and 3.5 eV compared to 3.9 eV calculated from direct transitions.

4. Conclusion

SnO_2–ZnO film composite nanomaterials with high transparency in the visible wavelength range were obtained by low-temperature solid-phase pyrolysis. X-ray analysis showed the existence of two oxide materials phases — in the form of wurtzite and cassiterite. The average particle size of synthesized composite materials was calculated, and the activation energy of the conductivity is determined, which correlates with each other and affects specific conductivity. Studies of optical absorption spectra have shown that an absorption of photons for all synthesized materials was observed not only due to direct transitions, but also due to indirect transitions. The band gap determined from the self-absorption at direct transitions (E_{g1}) showed a traditional increase from 3.32 to 3.90 eV with an increase in the amount of tin oxide from 5% to 95%. The intrinsic absorption at indirect transitions resulted from the nanoscale structure of films with average crystallite sizes from 8 to 16 nm. The band gap determined from the intrinsic absorption at indirect transitions (E_{g2}) for all the synthesized materials was significantly smaller than the band gap determined for direct transitions. A minimum E_{g2} value of 2.998 eV was observed for a $50SnO_2$–$50ZnO$ film, which has minimal nanocrystallite sizes. The existence of a large number of heterojunctions between nanocrystallites formed by different oxides suggests the presence of a surface electric field with a strength higher than 4×10^5 V/cm, which also affects the shift in optical absorption and a decrease in the E_{g2} value.

References

[1] Z. Wang, P. K. Nayak, J. A. Caraveo-Frescas and H. N. Alshareef, Recent developments in p-type oxide semiconductor materials and devices, *Adv. Mater.* **28**(20), 3831 (2016).

[2] X. X. Han, W. Ji, B. Zhao and Y. Ozaki, Semiconductor-enhanced Raman scattering: Active nanomaterials and applications, *Nanoscale* **9**(15), 4847 (2017).

[3] E. M. Bayan, T. G. Lupeiko, L. E. Pustovaya and M. G. Volkova, Synthesis and photocatalytic properties of Sn–TiO_2 nanomaterials, *J. Adv. Dielectr.* **10**(1–2), 2060018 (2020).

[4]V. V. Petrov, E. M. Bayan, S. A. Khubezhov, Y. N. Varzarev and M. G. Volkova, Investigation of rapid gas-sensitive properties degradation of ZnO–SnO$_2$ thin films grown on the glass substrate, *Chemosensors* **8**(2), 40 (2020).

[5]J. Song, E. Zheng, X.-F. Wang, W. Tian and T. Miyasaka, Low-temperature-processed ZnO–SnO$_2$ nanocomposite for efficient planar perovskite solar cells, *Sol. Energy Mater. Sol. Cells* **144**, 623 (2016).

[6]P. Tiwana, P. Docampo, M. B. Johnston, H. J. Snaith and L. M. Herz, Electron mobility and injection dynamics in mesoporous ZnO, SnO$_2$, and TiO$_2$ films used in dye-sensitized solar cells, *ACS Nano* **5**(6), 5158 (2011).

[7]L. Luo, W. Xu, Z. Xia, Y. Fei, J. Zhu, C. Chen, Y. Lu, Q. Wei, H. Qiao and X. Zhang, Electrospun ZnO–SnO$_2$ composite nanofibers with enhanced electrochemical performance as lithium-ion anodes, *Ceram. Int.* **42**(9), 10826 (2016).

[8]S. V. P. Vattikuti, P. A. K. Reddy, J. Shim and C. Byon, Visible-light-driven photocatalytic activity of SnO$_2$–ZnO quantum dots anchored on g-C$_3$N$_4$ nanosheets for photocatalytic pollutant degradation and H$_2$ production, *ACS Omega* **3**(7), 7587 (2018).

[9]S. Lee, C. Hwang, J. Pi, M. Ryu, H. Oh, S. H. Cho, J. Yang, S. Ko, P. Hye and Y. Chu, Characterization of ZnO–SnO$_2$ nanocomposite thin films deposited by pulsed laser ablation and their field effect electronic properties, *Mater. Lett.* **122**, 94 (2014).

[10]V. V. Petrov, Y. N. Varzarev, E. M. Bayan, V. Y. Storozhenko and A. A. Rozhko, Study of the electrophysical properties of thin films of mixed zinc and tin oxides, *Proc. 2019 IEEE Int. Conf. Electrical Engineering and Photonics*, Vol. 8906834, (2019), pp. 242–243.

[11]G. Korotcenkov and B.K. Cho, Metal oxide composites in conductometric gas sensors: Achievements and challenges, *Sens. Actuators B Chem.* **244**, 182 (2017).

[12]L. Zhu and W. Zeng, Room-temperature gas sensing of ZnO-based gas sensor: A review, *Sens. Actuators A* **267**, 242 (2017).

[13]J. Fang, Y. Zhu, D. Wu, C. Zhang, S. Xu, D. Xiong, P. Yang, L. Wang and P. K. Chu, Gas sensing properties of NiO/SnO$_2$ heterojunction thin film, *Sens. Actuators B Chem.* **252**, 1163 (2017).

[14]T. Lia, W. Zenga and Z. Wang, Quasi-one-dimensional metal-oxide-based heterostructural gas-sensing materials: A review, *Sens. Actuators B* **221**, 1570 (2015).

[15]A. Mirzaei, S. G. Leonardi and G. Neri, Detection of hazardous volatile organic compounds (VOCs) by metal oxide nanostructures-based gas sensors: A review, *Ceram. Int.* **42**, 15119 (2016).

[16]Y. Nakanishi, K. Kato, M. Horikawa and M. Yonekura, Influence of Zn–Sn ratio on optical property and microstructure of Zn–Sn–O films deposited by magnetron sputtering, *Thin Solid Films* **612**, 231 (2016).

[17]V. K. Jain, P. Kumar, M. Kumar, P. Jain, D. Bhandari and Y. K. Vijay, Study of post annealing influence on structural, chemical and electrical properties of ZTO thin films, *J. Alloys Compd.* **509**(8), 3541 (2011).

[18]T. Tharsika, A. S. M. A. Haseeb and M. F. M. Sabri, Structural and optical properties of ZnO–SnO$_2$ mixed thin films deposited by spray pyrolysis, *Thin Solid Films* **558**, 283 (2014).

[19]A. B. Khatibani, S. M. Rozati and Z. A. Hallaj, Synthesis and characterization of nanostructure CdO:Zn thin films deposited by spray pyrolysis technique: Molarity and heat treatment effects, *Mater. Sci. Semicond. Process.* **16**(3), 980 (2013).

[20]F. Atay, I. Akyuz, D. Durmaz and S. Kose, Characterization of ZnO-SnO$_2$ oxide systems produced by ultrasonic spray pyrolysis, *Sol. Energy* **193**, 666 (2019).

[21]J-C. Li, X-Y. Hou and Q. Cao, Effect of Zn/Sn ratio on structure and properties of ZnO–SnO$_2$ nanocomposite films, *J. Alloys Compd.* **611**, 219 (2014).

[22]H.-L. Yuan and J.-C. Li, Effect of annealing temperature on the growth of Zn-Sn-O nanocomposite thin films, *J. Alloys Compd.* **714**, 114 (2017).

[23]S.-M. Lee, Y.-H. Joo and C.-I. Kim, Influences of film thickness and annealing temperature on properties of sol–gel derived ZnO–SnO$_2$ nanocomposite thin film, *Appl. Surf. Sci.* **320**, 494 (2014).

[24]G. H. Lee, Y. Yamamoto, M. Kourogi and M. Ohtsu, Blue shift in room temperature photoluminescence from photo-chemical vapor deposited ZnO films, *Thin Solid Films* **386**(1), 117 (2001).

[25]D. Y. Torres Martínez, R. Castanedo Pérez, G. Torres Delgado and O. Zelaya Ángel, Structural, morphological, optical and photocatalytic characterization of ZnO–SnO$_2$ thin films prepared by the sol–gel technique, *J. Photochem. Photobiol. A Chem.* **235**, 49 (2012).

[26]M. Bagheri-Mohagheghi and M. Shokooh-Saremi, The electrical, optical, structural and thermoelectrical characterization of *n*- and *p*-type cobalt-doped SnO$_2$ transparent semiconducting films prepared by spray pyrolysis technique, *Physica B* **405**(19), 4205 (2010).

[27]B. Xu, X.-G. Ren, G.-R. Gu, L.-L. Lan and B.-J. Wu, Structural and optical properties of Zn-doped SnO$_2$ films prepared by DC and RF magnetron co-sputtering, *Superlattices Microstruct.* **89**, 34 (2016).

[28]M. G. Volkova, V. Y. Storozhenko, V. V. Petrov and E. M. Bayan, Characterization of nanocrystalline ZnO thin films prepared by new pyrolysis method, *J. of Phys. Conf. Ser.* **1695**(1), 012023 (2020).

[29]V. V. Petrov, V. V. Sysoev, A. P. Starnikova, M. G. Volkova, Z. K. Kalazhokov, V. Y. Storozhenko, S. A. Khubezhov and E.M. Bayan, Synthesis, Characterization and Gas Sensing Study of ZnO-SnO$_2$ Nanocomposite Thin Films. *Chemosensors*, **9**(6), 124 (2021).

[30]V. V. Petrov, A. P. Starnikova, Y. N. Varzarev, K. A. Abdullin and D. P. Makarenko, Gas sensitive properties of ZnO nanorods formed on silicon and glass substrates, *IOP Conf. Ser. Mater. Sci. Eng.* **703**, 012038 (2019).

[31]K. V. Shalimova, *Physics of Semiconductors* (Energia, Moscow, 1976).

[32]M. Schreyer, L. Guo, S. Thirunahari, F. Gao and M. Garland, Simultaneous determination of several crystal structures from powder mixtures: The combination of powder X-ray diffraction, band-target entropy minimization and Rietveld methods, *J. Appl. Crystallogr.* **47**(2), 659 (2014).

[33]M. Klementova, Z. Weiss and M. Rieder, Rietveld refinement of cassiterite: A caveat for meticulous sample preparation, *Int. J. Inorg. Mater.* **45**(1), 155 (2000).

[34]S. I. Rembeza, T. V. Svistova, E. S. Rembeza and O. I. Borsyakova, Microstructure and physical properties of SnO$_2$ thin films, *Phys. Technol. Semicond.* **35**(7), 796 (2001).

[35]F. Urbach, The long-wavelength edge of photographic sensitivity and of the electronic absorption of solids, *Phys. Rev.* **92**, 1324 (1953).

[36]Z. Yang, K. P. Homewood, M. S. Finney, M. A. Harry and K. J. Reeson, Optical absorption study of ion beam synthesized polycrystalline semiconducting FeSi$_2$, *J. Appl. Phys.* **78**, 1958 (1995).

[37]R. Singh and T. Som, Direct evidence of band-bending at grain boundaries of ZnO:SnO$_2$ films: Local probe microscopic studies, *Sol. Energy* **208**, 275 (2020).